Dyes and Pigments 216 (2023) 111349

Contents lists available at ScienceDirect

Dyes and Pigments

journal homepage: www.elsevier.com/locate/dyepig

Short communication

Hole-transport materials based on benzodithiophene-thiazolothiazole-containing conjugated polymers for efficient perovskite solar cells

M.M. Tepliakova [a], I.E. Kuznetsov [b], D.S. Zamoretskov [b,c], A.N. Zhivchikova [b,a], A.V. Lolaeva [b], A.D. Furasova [d], M.A. Sandzhieva [d], S.V. Makarov [d,e], M.V. Klyuev [c], D.K. Sagdullina [b], E.O. Perepelitsina [b], Y.G. Gladush [a], A.G. Nasibulin [a], K.J. Stevenson [f], A.V. Akkuratov [b,*]

[a] Skolkovo Institute of Science and Technology, Bolshoi bld., 30, b. 1, Moscow, 121205, Russian Federation
[b] Federal Research Center of Problems of Chemical Physics and Medicinal Chemistry, Russian Academy of Sciences. FRC PCPMC RAS, Academician Semenov avenue 1, Chernogolovka, 142432, Russian Federation
[c] Ivanovo State University, 153025, Ivanovo, Russian Federation
[d] School of Physics and Engineering, ITMO University, St. Petersburg, Russian Federation
[e] Qingdao Innovation and Development Center, Harbin Engineering University, Qingdao, 266000, Shan-dong, China
[f] Department of Chemistry, Moscow State University, 119992, Moscow, Russian Federation

ARTICLE INFO

Keywords:
Perovskite solar cells
Hole-transport materials
Conjugated polymers
Triisopropylsilyl chains
Benzodithiophene

ABSTRACT

Conjugated polymers are promising hole-transport materials (HTMs) for designing efficient and stable perovskite solar cells (PSCs). The structure of polymer backbone and position of side substituents greatly influences their electronic properties, film morphology, and hence, the charge extraction and charge transport characteristics of HTMs. Herein, we design two novel donor-acceptor conjugated polymers based on benzodithiophene (BDT) bearing triisopropylsilyl substituents and thiophene-flanked thiazolothiazole block (Tz) with different side chain position. In polymer **in-BDTTz** alkyl chains are placed "toward" to the Tz moiety, while in **aus-BDTTz** "outward" to the Tz block. Polymeric HTM **in-BDTTz** enables 18.7% power conversion efficiency in devices outperforming that of PSCs with **aus-BDTTz** and reference devices employing poly(triarylamine) (PTAA). Furthermore, PSCs with **in-BDTTz** as HTM demonstrates stable operation comparable to that of PTAA-based devices. These findings feature alkylsilyl-substituted benzodithiophene-based polymers as promising dopant-free hole-transport materials for efficient and stable perovskite photovoltaics.

1. Introduction

Conjugated polymers are promising semiconductor materials for the next-generation electronic devices such as organic solar cells [1], photodetectors [2], organic field-effect transistors [3] and sensors [4]. In the recent years, conjugated polymers are also extensively investigated as charge transport materials for perovskite solar cells (PSCs) [5]. PSCs attract great attention because of high power conversion efficiencies (PCEs) approaching 26% [6] and easy fabrication of devices by printing techniques (slot-die coating, inkjet printing etc.) [7]. These advantages make PSCs potentially capable to supplant silicon-based solar cells in the market. However, lagging behind in reaching long-term operation stability of PSCs hinder their commercialization [8]. One of the efficient ways to stabilize devices lies in introducing organic semiconductors as charge transport materials [9–13]. Employing of polymeric hole-transport materials (HTMs) with fine-tuned energy levels in PSCs ensures selective hole extraction, prevents direct contact between perovskite absorbers and metal electrode, and protects perovskite layer from moisture ingress due to hydrophobic nature of organic compounds [14]. Therefore, design of dopant-free polymeric HTMs with high charge transport characteristics, good energy level alignment with valence band of perovskite, and high photo- and thermal stability is an important benchmark for development of efficient and stable PSCs.

Previously, benzodithiophene-based (BDT) conjugated polymers were shown to be promising HTMs for perovskite solar cells [15,16]. Incorporation of BDT building block with high planarity and symmetry

* Corresponding author.
E-mail address: akkuratow@yandex.ru (A.V. Akkuratov).

https://doi.org/10.1016/j.dyepig.2023.111349
Received 28 February 2023; Received in revised form 21 April 2023; Accepted 23 April 2023
Available online 28 April 2023

into polymer backbone was found beneficial for achieving high charge carrier mobility [17,18]. Furthermore, functionalization of BDT in positions 4 and 8 by various heteroaryl or alkyl substituents enables additional tuning of optoelectronic and physicochemical properties of resulting polymers such as energy of highest occupied molecular orbital (HOMO), lowest unoccupied molecular orbital (LUMO) and solubility. In our recent work, we demonstrated that BDT-based polymer **BDT-BTB** comprising R_3Si- side groups (Fig. 1) exhibited better film-forming ability and higher hole mobilities as compared to analogues with alkyl or alkoxy chains. Using **BDT-BTB** as HTM in PSCs enabled encouraging PCEs of 17.4% [19].

In this work, we report on synthesis of two novel conjugated polymers **in-BDTTz** and **aus-BDTTz** containing triisopropylsilyl-substituted benzodithiophene block and thiophene-flanked thiazolothiazole (Tz) moiety and its investigation as HTM for n-i-p perovskite solar cells (Fig. 1). The electron-deficient thiazolothiazole attracts much interest due to straightforward synthesis of donor-acceptor polymers with high charge-transport characteristics [20,21], high oxidative stability [22,23], good thermo- and photostability [24,25], which is very important for efficient and long-term operation of PSCs. Since the position of alkyl side chains might strongly influence the charge transport properties of polymers [26–28], we additionally varied the placement of 2-ethylhexyl substituents on thiophene rings to investigate this effect for designed polymers.

PSCs with **in-BDTTz** as HTM delivered high PCEs approaching 19%, thus demonstrating great potential of polymers with alternating benzodithiophene and thiazolothiazole building blocks for high-performance of perovskite photovoltaics.

2. Results and discussion

The synthesis of key monomer **M1** and conjugated polymers **in-BDTTz** and **aus-BDTTz** is shown in Fig. 2. The thiazolothiazole-based monomers **M2** and **M3** were prepared according to previously reported methods [29,30].

First, thiophene-3-carboxylic acid was treated with thionyl chloride affording thiophene-3-carbonyl chloride. The reaction of compound **1** with diethylamine in methylene chloride gave *N,N*-diethylthiophene-3-carboxamide **2**, which was treated with n-butyllithium followed by quenching of intermediate with water. The reaction of formed benzo[1,2-*b*:4,5-*b'*]dithiophene-4,8-dione **3** with (5-(triisopropylsilyl)thiophen-2-yl)lithium **5** followed by reduction of the corresponding diol with tin (II) chloride in hydrochloric acid produced compound **6**. The monomer **M1** was obtained by lithiation of **6** with *n*-BuLi in THF and treatment of dilithiated derivative with trimethylchlorostannane. The Stille polycondensation reaction between monomers **M1** and **M2** or **M3** resulted in conjugated polymers **in-BDTTz** and **aus-BDTTz.** The detailed synthetic procedures are described in the Supporting Information. Additionally, we estimated the cost of synthesis of the polymers according to the previously reported calculation model [9]. The cost of both polymers (*ca.* 307 $/g) is lower than that of the state-of-the-art PTAA HTM (423 $/g).

In order to remove low molecular weight impurities, polymers **in-BDTTz** and **aus-BDTTz** were washed in the Soxhlet apparatus with hexane, acetone, chloroform and chlorobenzene followed by concentration of the chlorobenzene fractions and precipitation of the polymer with ethanol. The molecular weight characteristics of polymers were determined by gel permeation chromatography relative to polystyrene standards. The weight-average molecular weights (M_w) of **in-BDTTz** and **aus-BDTTz** were estimated as 213 kDa and of 151 kDa, respectively (Table 1). Polymers showed moderate solubility in chlorobenzene (CB) and 1,2-dichlorobenzene (DCB) at room temperature. Thermal properties of polymers were investigated using thermogravimetry (TGA, Fig. 3a) and differential scanning calorimetry (DSC).

As can be seen from Fig. 3, both polymers exhibited high thermal stability with decomposition temperature above 400 °C that is much higher than temperatures of the fabrication and operation conditions of PSCs. DSC measurements (Fig. S1, Supporting Information) showed that there are no thermal transitions upon heating and cooling cycles implying low crystallinity of polymers in the solid-state. Thus good morphological stability of HTM films can be expected under operation conditions of PSCs.

Optical properties of conjugated polymers were investigated using absorption spectroscopy and photoluminescence (PL) spectroscopy (Fig. 3b). The optical properties of **in-BDTTz** in diluted 1,2-dichlorobenzene solution and in films are very similar (Fig. S2).

The solution of **in-BDTTz** exhibited two major absorption maxima of 541 nm and 579 nm, whereas the maxima for polymer film are located at 535 nm and 580 nm (Table 1, Fig. S2). A negligible spectral shift of long-wavelength band when going from solution to solid state might be due to aggregation of macromolecules in solution at room temperature. On the contrary, **aus-BDTTz** demonstrated a noticeable bathochromic shift of 44 nm implying the self-ordering of polymer chains in films. The emission bands in photoluminescence (PL) spectra exhibited similar red-shift to absorption bands. PL maxima are located at 622 and 673 nm for **in-BDTTz**, and at 618 nm and 673 nm for **aus-BDTTz**. The small Stokes shifts of 987.7 cm^{-1} for **in-BDTTz** and 1331.9 cm^{-1} for **aus-BDTTz** reveal a minor structural difference between the excited and ground states of polymers as well as low reorganization energy of the polarons, which limits the intrinsic mobility of semiconductor molecules [31,32]. The optical bandgap of polymers were calculated as $E_{gap}^{opt} = 1241/\lambda_{int}^{film}$, where λ_{int}^{film} is wavelength at intersection of absorption and PL bands. As can be seen, E_{gap}^{opt} values of **in-BDTTz** and **aus-BDTTz** are almost the same (*ca.* 2.1 eV).

The energies of frontier molecular orbitals of polymers were estimated from cyclic voltammetry measurements of thin films (CV, Fig. 3c). The energies of the highest occupied molecular orbital were

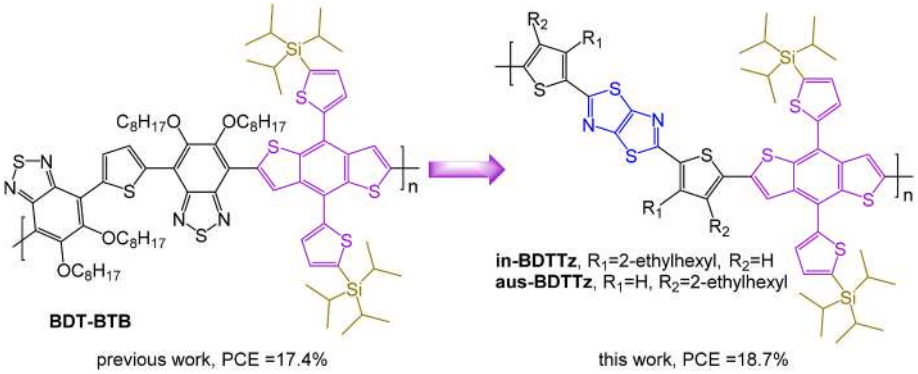

Fig. 1. Structures of conjugated polymers **BDT-BTB** from the previous work [19], and **in-BDTTz** and **aus-BDTTz** obtained in this work.

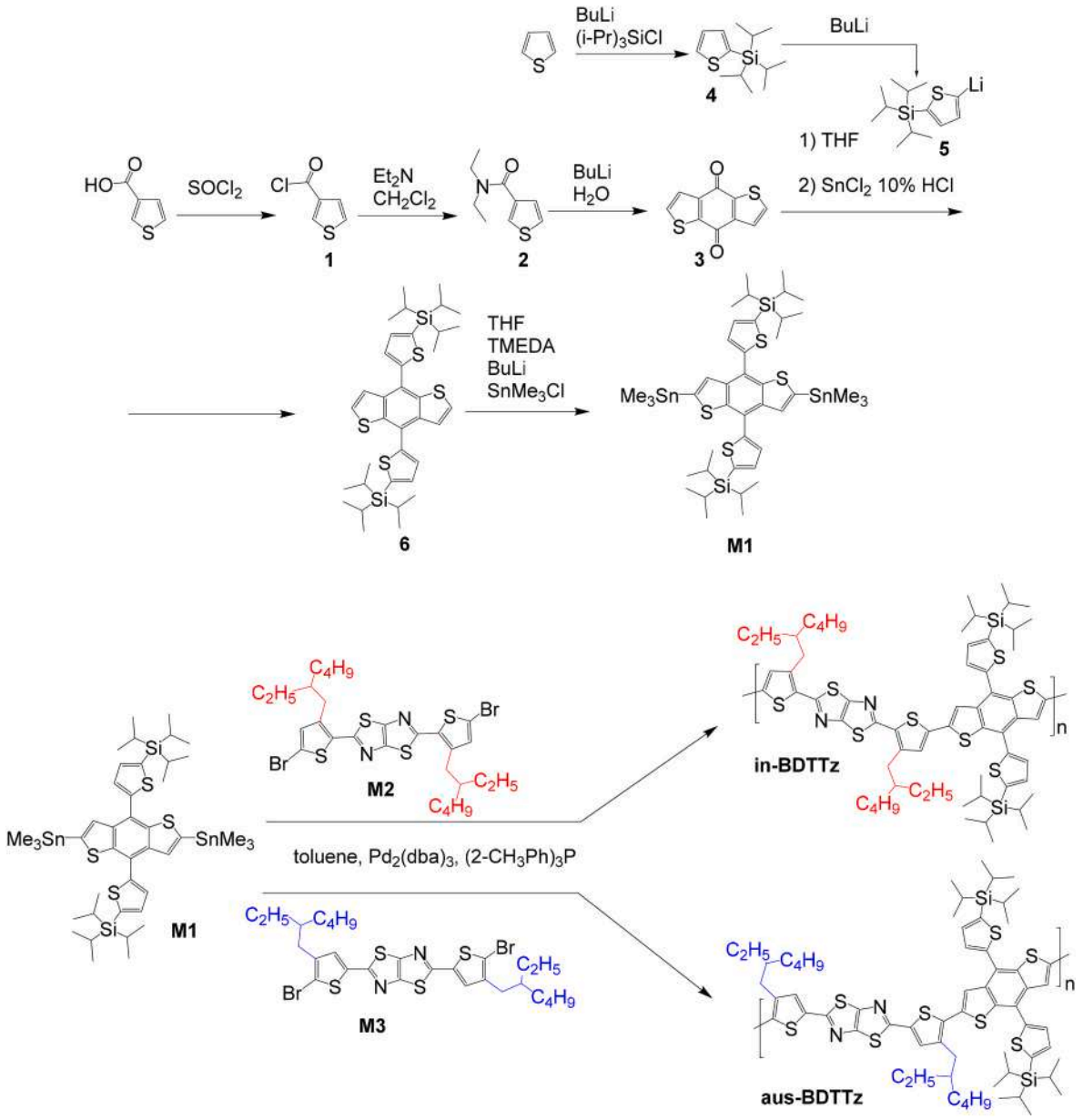

Fig. 2. Synthesis of monomer **M1** and conjugated polymers **in-BDTTz** and **aus-BDTTz**.

Table 1
Physicochemical, optical, and electrochemical properties of polymers **in-BDTTz** and **aus-BDTTz**.

Polymer	M_w, kDa(M_w/M_n)	λ_{max}^{sol}/ λ_{max}^{film}, nm	λ_{max}^{PL}, nm	E_{gap}^{opt}, eV	HOMO, eV	LUMO, eV	T_d, °C	μ_h, $cm^2V^{-1}s^{-1}$
in-BDTTz	213(2.1)	579/538,586	622,673	2.05	−5.16	−3.11	429	2.81×10^{-4}
aus-BDTTz	151(3.2)	527/535,571	618,673	2.07	−5.26	−3.19	435	2.14×10^{-4}

determined as HOMO $= -e(E_{onset}^{ox} + 4.8)$ eV, where E_{onset}^{ox} is onset oxidation potential and 4.8 eV is absolute redox potential of ferrocene/ferrocenium couple *vs.* vacuum level [33]. Oxidation potentials were found to be 0.4 V for **in-BDTTz** and 0.5 V for **aus-BDTTz**. Assuming that $E_{1/2}$ of the Fc/Fc^+ redox couple was 0.043 V versus $Ag/AgNO_3$ reference electrode, the HOMO energies were found to be −5.16 eV and −5.26 eV for **in-BDTTz** and **aus-BDTTz**, respectively (Table 1). Since no reduction peaks were registered on CV curves, the energies of the lowest unoccupied molecular orbital (LUMO) were calculated from energy bandgap and HOMO energies as E_{gap}^{opt} +HOMO. With respect to the valence band of perovskite (−5.4 eV for $CH_3NH_3PbI_3$ or $MAPbI_3$ [34]), HOMO energy levels of both polymers are suitable for extraction of photogenerated holes from $MAPbI_3$. At the same time, the estimated LUMO levels lie higher than conduction band of $MAPbI_3$ (−3.9 eV) to prevent electron transfer to hole-collecting electrode. The energy level diagram of used materials in the PSCs is depicted in Fig. 3d.

Hole mobilities (μ_h) of **in-BDTTz** and **aus-BDTTz** were measured by space charge limited current (SCLC) technique in hole-only devices with a structure of ITO/PEDOT:PSS/Polymer/MoO_3/Ag. The μ_h values were calculated from the Mott-Gurney square law $J = (9/8)\varepsilon_0\varepsilon_r\mu_h(V^2/L^3)$, where ε_0 is vacuum permittivity, ε_r is the dielectric constant of polymers (generally, 3.0–3.5 for organic semiconductors), μ_h is the hole mobility,

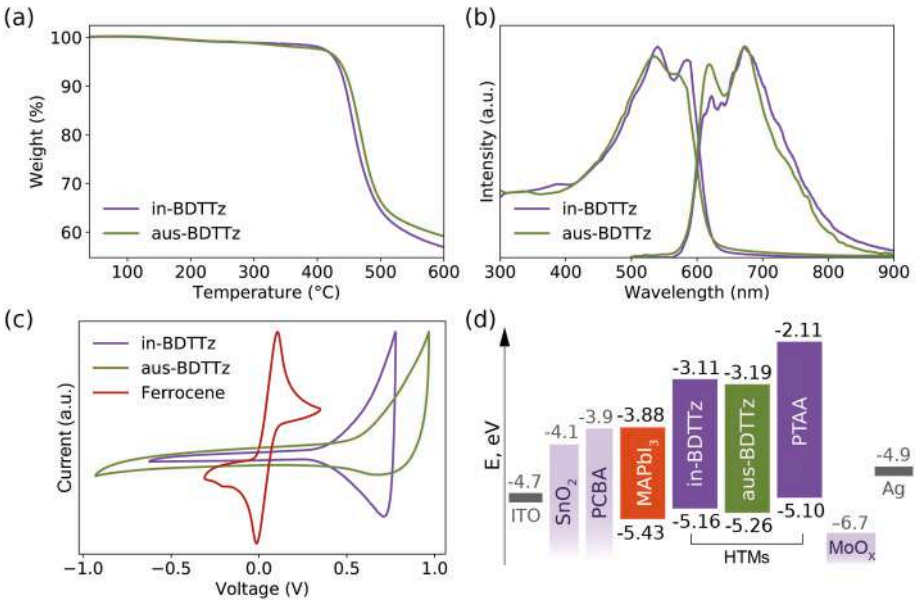

Fig. 3. TGA curves measured in inert atmosphere (a); Absorption and PL spectra (b), and CV curves (c) of polymers in thin films; energy level diagram (d).

V is the effective applied voltage, and L is the thickness of polymer films. The obtained hole mobilities of 2.81 × 10^{-4} $cm^2V^{-1}s^{-1}$ for **in-BDTTz** and of 2.14 × 10^{-4} $cm^2V^{-1}s^{-1}$ is for **aus-BDTTz**, which is higher than that of state-of-the-art HTM PTAA [35].

At the next step, conjugated polymers **in-BDTTz** and **aus-BDTTz** were investigated as hole transport materials in PSCs with n-i-p configuration. The details of PSCs fabrication are provided in the Supporting Information. Briefly, the ITO substrates were covered with SnO_2 followed by passivation with the fullerene derivative phenyl-C_{61}-butyric acid [36]. The photoactive perovskite layer $MAPbI_3$ was deposited atop in an inert atmosphere. Then, polymeric HTMs **in-BDTTz** or **aus-BDTTz** were spin-coated from chlorobenzene solution. Finally, the MoO_x and the silver electrode were thermally evaporated under vacuum, resulting in the architecture of ITO/SnO_2:PCBA(15 nm)/$MAPbI_3$(300 nm)/**HTM** (15 nm)/MoO_x(20 nm)/Ag(100 nm). The optimal deposition conditions for each HTM were estimated in preliminary experiments and were found to be the same for both materials: spin-coating of 7 mg mL^{-1} warm solution (60°) of the undoped polymer at 5000 rpm. The *J*-V curves and EQE spectra of the best devices are presented in Fig. 4, and

Table 2
Photovoltaic performance of PSCs based on **PTAA**, **in-BDTTz** and **aus-BDTTz**.

HTM	V_{OC}, mV	J_{SC}, mA cm^{-2}	FF,%	PCE,%
PTAA	1040[a](1040 ± 30)[b]	21.8(21.4 ± 0.3)	77.5(74.8 ± 6.1)	17.4(16.6 ± 1.7)
in-BDTTz	1060(1060 ± 10)	22.5(22.2 ± 0.2)	79.1(77.4 ± 4.6)	18.7(18.4 ± 0.2)
aus-BDTTz	1080(1070 ± 10)	21.9(21.0 ± 0.4)	67.0(66.0 ± 1)	15.7(15.2 ± 0.4)

[a] Maximal value (average ± standard deviation).
[b] Average characteristics for sixteen devices.

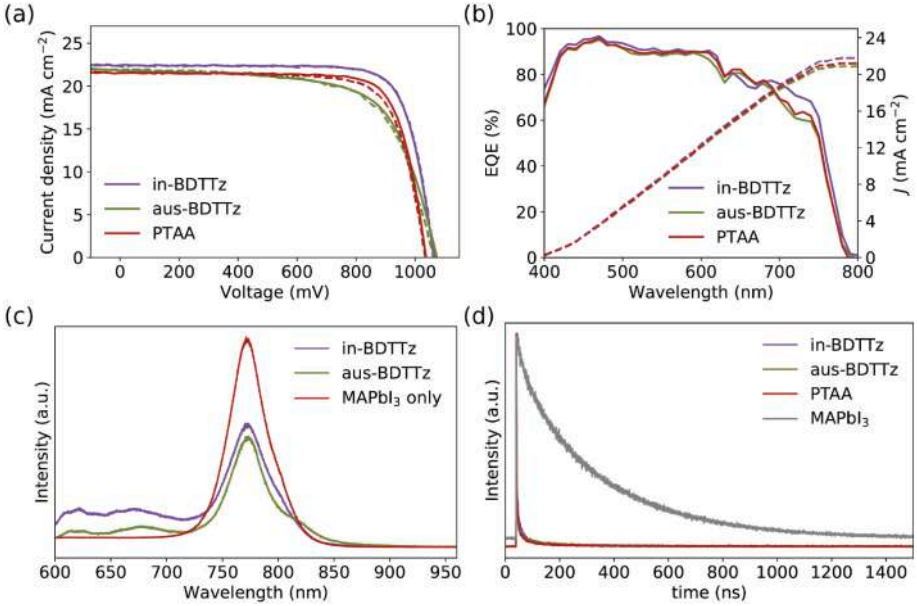

Fig. 4. *J*-V curves for best devices with different HTMs. Solid lines correspond to forward scans and dashed lines correspond to reverse scans (a); EQE spectra (b); steady-state PL spectra for films of polymers (c) and TRPL spectra for glass/perovskite/HTM stacks (d).

the parameters of PSCs are summarized in Table 2. The photovoltaic parameters of PSCs obtained from reverse scans are presented in Table S1 (Supporting Information).

PSCs with **in-BDTTz** outperformed devices with **aus-BDTTz** and with the reference polymer **PTAA**. The best devices exhibited power conversion efficiencies of 18.7% with open-circuit voltages (V_{OC}) of 1.06 V, short-circuit current densities (J_{SC}) of 22.5 mA cm^{-2} and fill factors (FF) of 79%. The J_{SC} values from *J*–V curves of the corresponding PSCs are in agreement with the J_{SC} values calculated from the integration of EQE spectra (Fig. 4a). Interestingly, the highest open-circuit voltages were obtained for PSCs with **aus-BDTTz**. The reason for this is probably better energy level alignment between the HOMO of this material and the perovskite valence band. Nevertheless, the highest short-circuit currents and fill factors were registered for devices comprising **in-BDTTz** thus justifying good charge transfer characteristics of this material as well as good electrical contact with the perovskite layer.

To evaluate the hole extraction ability of obtained polymers, steady-state photoluminescence (PL) and time-resolved photoluminescence (TRPL) spectra of bilayer structures with configuration perovskite/HTM were performed.

The observed PL quenching of samples was of the same intensity, while a slightly stronger quenching can be seen for **aus-BDTTz** (Fig. 4c). The TRPL data supports the results showing low charge carrier lifetime in perovskite covered with developed HTMs (Fig. 4d). It should be mentioned that a shoulder related to the internal photoluminescence of polymers contributes to the shape of TRPL decay curves.

In the next step, we investigated the surface of polymer films using contact angle measurements (Fig. 5a).

The contact angle of water on polymer films exceeded 90°, revealing the highly hydrophobic nature of the polymer films. This allows the expectation of good protection of the perovskite layer from the moisture ingress when covered with BDTTz materials. The height profile of the polymer films was also characterized. According to atomic force microscopy (AFM) measurements, the film **aus-BDTTz** contains a sufficient amount of larger formations on the surface implying different aggregation behavior of polymers. The root-mean-square roughness for films based on **in-BDTTz** and **aus-BDTTz** were found to be 2.23 nm and 3.57 nm, respectively.

Additionally, the operation stability of devices containing the best performing material **in-BDTTz** was investigated under continuous illumination of LED light in an inert atmosphere (75 $mWcm^{-2}$; O_2 and H_2O < 0.1 ppm; 45 °C). Encouragingly, almost no PCE loss for devices was found. Indeed, after the short burn-in period, the efficiency of both **in-BDTTz-** and **PTAA**-based PSCs stabilized and remained unchanged after 375 h of continuous operation (Fig. S3). All of the results demonstrated that the novel polymers comprising alternating benzodithiophene and thiazolothiazole building blocks are favorable to improve the device performance as well as stability, which provides new guidelines for HTM designing strategies.

3. Conclusion

In this work, we have successfully designed two novel polymeric hole-transport materials by modification of our previously synthesized benzodithiophene-benzothiadiazole-based conjugated polymers. Introduction of the thiazolothiazole motif into backbone of polymers had a positive effect on their thermal stability, charge-transport characteristics and energy levels alignment with valence band of perovskite. The variation of 2-ethylhexyl side chains position on thiophene ring did not significantly affect the optical or physicochemical properties of polymers, though distinctly influence the HOMO level energies and hole mobilities. Polymer **in-BDTTz**, where the alkyl chains were placed "toward" the Tz moiety provided higher charge mobilities that resulted in enhanced performance of PSCs. Devices incorporating **in-BDTTz** HTMs delivered PCEs approaching 19% and stable performance under continuous illumination underlying the importance of molecular design for improving efficiency and stability of perovskite solar cells.

CRediT authorship contribution statement

M.M. Tepliakova: Investigation, Writing – review & editing. **I.E. Kuznetsov:** Investigation. **D.S. Zamoretskov:** Formal analysis. **A.N. Zhivchikova:** Investigation. **A.V. Lolaeva:** Investigation. **A.D. Furasova:** Investigation. **M.A. Sandzhieva:** Investigation. **S.V. Makarov:** Investigation. **M.V. Klyuev:** Writing – review & editing. **D.K.**

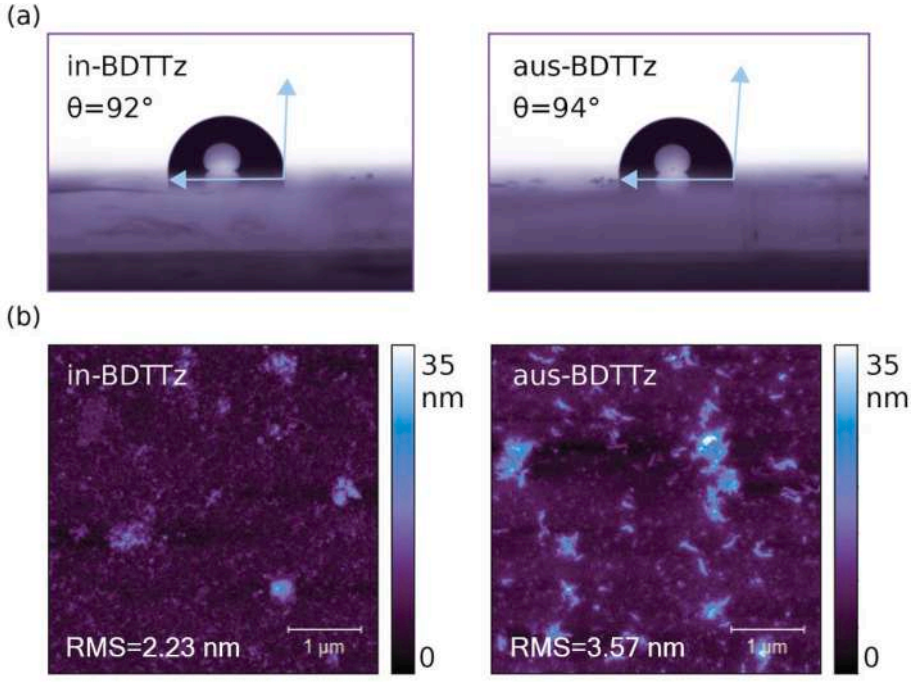

Fig. 5. Contact angle of water on polymer films (a); AFM images of polymer films (b).

Sagdullina: Investigation. **E.O. Perepelitsina:** Formal analysis. **Y.G. Gladush:** Investigation. **A.G. Nasibulin:** Investigation. **K.J. Stevenson:** Supervision, Writing – review & editing. **A.V. Akkuratov:** Conceptualization, Supervision, Writing – review & editing.

Declaration of competing interest

The authors declare that they have no known competing financial interests or personal relationships that could have appeared to influence the work reported in this paper.

Data availability

No data was used for the research described in the article.

Acknowledgments

This work was funded by Russian Science Foundation (grant no. 21-73-10182). This work was performed using the equipment of the Research Center FRC PCPMC RAS. AFM and TRPL measurements were funded by Skolkovo Institute of Science and Technology (grant 1-NGP-1487).

Appendix A. Supplementary data

Supplementary data to this article can be found online at https://doi.org/10.1016/j.dyepig.2023.111349.

References

[1] Xia D, Li C, Li W. Crystalline conjugated polymers for organic solar cells: from donor, acceptor to single-component. Chem Rec 2019;19:962–72. https://doi.org/10.1002/tcr.201800131.
[2] Zhu D, Ji D, Li L, Hu W. Recent progress in polymer-based infrared photodetectors. J Mater Chem C 2022;10:13312–23. https://doi.org/10.1039/D2TC00646D.
[3] Kimpel J, Michinobu T. Conjugated polymers for functional applications: lifetime and performance of polymeric organic semiconductors in organic field-effect transistors. Polym Int 2021;70:367–73. https://doi.org/10.1002/pi.6020.
[4] Ohayon D, Inal S. Organic bioelectronics: from functional materials to next-generation devices and power sources. Adv Mater 2020:2001439. https://doi.org/10.1002/adma.202001439.
[5] Xiao Q, Tian J, Xue Q, Wang J, Xiong B, Han M, Li Zh, Zhu Z, Yip H, Li Z. Dopant-free squaraine-based polymeric hole-transporting materials with comprehensive passivation effects for efficient all-inorganic perovskite solar cells. Angew Chem Int Ed 2019;58:17724–30. https://doi.org/10.1002/anie.201907331.
[6] Zhang H, Ji X, Yao H, Fan Q, Yu B, Li J. Review on efficiency improvement effort of perovskite solar cell. Sol Energy 2022;233:421–34. https://doi.org/10.1016/j.solener.2022.01.060.
[7] Zi W, Jin Z, Liu S, Xu B. Flexible perovskite solar cells based on green, continuous roll-to-roll printing technology. J Energy Chem 2018;27:971–89. https://doi.org/10.1016/j.jechem.2018.01.027.
[8] Duan L, Uddin A. Defects and stability of perovskite solar cells: a critical analysis. Mater Chem Front 2022;6:400–17. https://doi.org/10.1039/D1QM01250A.
[9] Xia Z, Zhang W, Chen C, Miao Y, Ding X, Wang L, Zhai M, Cheng M. Low-cost star-shaped hole-transporting materials with isotropic properties and its application in perovskite solar cells. Dyes Pigments 2022;207:110695. https://doi.org/10.1016/j.dyepig.2022.110695.
[10] Wang H, Zheng M, Chen C, Zhang W, Wang B, Yang C, Zhai M, Xu H, Cheng M. Electron transport interface engineering with pyridine functionalized perylene diimide-based material for inverted perovskite solar cell. Chem Eng J 2022;438:135410. https://doi.org/10.1016/j.cej.2022.135410.
[11] Zhai M, Wang A, Chen C, Hao F, Wang H, Ding L, Yang X, Cheng M. Construct efficient CsPbI2Br solar cells by minimizing the open-circuit voltage loss through controlling the peripheral substituents of hole-transport materials. Chem Eng J 2021;425:131675. https://doi.org/10.1016/j.cej.2021.131675.
[12] Ding X, Wang H, Chen C, Li H, Tian Y, Li Q, Cheng W, Ding L, Yang X, Cheng M. Passivation functionalized phenothiazine-based hole transport material for highly efficient perovskite solar cell with efficiency exceeding 22. Chem Eng J 2021;410:128328. https://doi.org/10.1016/j.cej.2020.128328.
[13] Girish KH, Vishnumurthy KA, Roopa TS. Role of conducting polymers in enhancing the stability and performance of perovskite solar cells: a brief review. Mater Today Sustain 2022;17:100090. https://doi.org/10.1016/j.mtsust.2021.100090.
[14] Zhang F, Yao Z, Guo Y, Li Y, Bergstrand J, Brett CJ, Cai B, Hajian A, Guo Y, Yang X, Gardner JM, Widengren J, Roth SV, Kloo L, Sun L. Polymeric, cost-effective, dopant-free hole transport materials for efficient and stable perovskite solar cells. J Am Chem Soc 2019;141. https://doi.org/10.1021/jacs.9b08424. 19700–7.
[15] Komissarova EA, Kuklin SA, Maskaev AV, Latypova AF, Kuznetsov PM, Emelianov NA, Nikitenko SL, Martynov IV, Kuznetsov IE, Akkuratov AV, Frolova LA, Troshin PA. Novel benzodithiophene-TTBTBTT copolymers: synthesis and investigation in organic and perovskite solar cells. Sustain Energy Fuels 2022;6:3542–50. https://doi.org/10.1039/D2SE00463A.
[16] Gaml EA, Dubey A, Reza KM, Hasan MN, Adhikari N, Elbohy H, Bahrami B, Zeyada H, Yang S, Qiao Q. Alternative benzodithiophene (BDT) based polymeric hole transport layer for efficient perovskite solar cells. Sol Energy Mater Sol Cells 2017;168:8–13. https://doi.org/10.1016/j.solmat.2017.04.002.
[17] Chen N-Y, Yue Q, Liu W, Zhang H-L, Zhu X. A benzo[1,2- *d* :4,5- *d* ′]bisthiazole-based wide-bandgap copolymer semiconductor for efficient fullerene-free organic solar cells with a small energy loss of 0.50 eV. J Mater Chem 2019;7:5234–8. https://doi.org/10.1039/C8TA11492G.
[18] Chen S, Jung S, Cho HJ, Kim N, Jung S, Xu J, Oh J, Cho Y, Kim H, Lee B, An Y, Zhang C, Xiao M, Ki H, Zhang Z, Kim J, Li Y, Park H, Yang C. Highly flexible and efficient all-polymer solar cells with high-viscosity processing polymer additive toward potential of stretchable devices. Angew Chem Int Ed 2018;57:13277–82. https://doi.org/10.1002/anie.201807513.
[19] Mikheeva AN, Kuznetsov IE, Tepliakova MM, Elakshar A, Gapanovich MV, Gladush YG, Perepelitsina EO, Sideltsev ME, Akhkiamova AF, Piryazev AA, Nasibulin AG, Akkuratov AV. Novel push-pull benzodithiophene-containing polymers as hole-transport materials for efficient perovskite solar cells. Molecules 2022;27:8333. https://doi.org/10.3390/molecules27238333.
[20] Guo B, Li W, Guo X, Meng X, Ma W, Zhang M, Li Y. High efficiency nonfullerene polymer solar cells with thick active layer and large area. Adv Mater 2017;29:1702291. https://doi.org/10.1002/adma.201702291.
[21] Cao Z, Chen J, Liu S, Qin M, Jia T, Zhao J, Li Q, Ying L, Cai Y-P, Lu X, Huang F, Cao Y. Understanding of imine substitution in wide-bandgap polymer donor-induced efficiency enhancement in all-polymer solar cells. Chem Mater 2019;31:8533–42. https://doi.org/10.1021/acs.chemmater.9b03570.
[22] Saito M, Osaka I, Suzuki Y, Takimiya K, Okabe T, Ikeda S, Asano T. Highly efficient and stable solar cells based on thiazolothiazole and naphthobisthiadiazole copolymers. Sci Rep 2015;5:14202. https://doi.org/10.1038/srep14202.
[23] Guo B, Guo X, Li W, Meng X, Ma W, Zhang M, Li Y. A wide-bandgap conjugated polymer for highly efficient inverted single and tandem polymer solar cells. J Mater Chem 2016;4:13251–8. https://doi.org/10.1039/C6TA04950H.
[24] Akkuratov AV, Nikitenko SL, Kozlov AS, Kuznetsov PM, Martynov IV, Tukachev NV, Zhugayevych A, Visoly-Fisher I, Katz EA, Troshin PA. Design of novel thiazolothiazole-containing conjugated polymers for organic solar cells and modules. Sol Energy 2020;198:605–11. https://doi.org/10.1016/j.solener.2020.01.087.
[25] Saito M, Osaka I. Impact of side chain placement on thermal stability of solar cells in thiophene–thiazolothiazole polymers. J Mater Chem C 2018;6:3668–74. https://doi.org/10.1039/C7TC04721E.
[26] Wan P, An C, Zhang T, Ma K, Liang N, Xu Y, Zhang S, Xu B, Zhang J, Hou J. The effect of aggregation behavior on photovoltaic performances in benzodithiophene-thiazolothiazole-based wide band-gap conjugated polymers with side chain position changes. Polym Chem 2020;11:1629–36. https://doi.org/10.1039/C9PY01438A.
[27] Saito M, Ogawa S, Osaka I. Contrasting effect of side-chain placement on photovoltaic performance of binary and ternary blend organic solar cells in benzodithiophene-thiazolothiazole polymers. ChemSusChem 2021;14:5032–41. https://doi.org/10.1002/cssc.202101345.
[28] Saito M, Osaka I. Impact of side chain placement on thermal stability of solar cells in thiophene–thiazolothiazole polymers. J Mater Chem C 2018;6:3668–74. https://doi.org/10.1039/C7TC04721E.
[29] Akpinar HZ, Udum YA, Toppare L. Spray-processable thiazolothiazole-based copolymers with altered donor groups and their electrochromic properties. J Polym Sci, Part A: Polym Chem 2013;51:3901–6. https://doi.org/10.1002/pola.26791.
[30] Cao Z, Chen J, Liu S, Qin M, Jia T, Zhao J, Li Q, Ying L, Cai Y-P, Lu X, Huang F, Cao Y. Understanding of imine substitution in wide-bandgap polymer donor-induced efficiency enhancement in all-polymer solar cells. Chem Mater 2019;31:8533–42. https://doi.org/10.1021/acs.chemmater.9b03570.
[31] Brusso JL, Hirst OD, Dadvand A, Ganesan S, Cicoira F, Robertson CM, Oakley RT, Rosei F, Perepichka DF. Two-dimensional structural motif in thienoacene semiconductors: synthesis, structure, and properties of tetrathienoanthracene isomers. Chem Mater 2008;20:2484–94. https://doi.org/10.1021/cm7030653.
[32] Mišicák R, Novota M, Weis M, Cigáň M, Šiffalovič P, Nádaždy P, Kožíšek J, Kožíšková J, Pavúk M, Putala M. Effect of alkyl side chains on properties and organic transistor performance of 2,6-bis(2,2′-bithiophen-5-yl)naphthalene. Synth Met 2017;233:1–14. https://doi.org/10.1016/j.synthmet.2017.08.010.
[33] Cardona CM, Li W, Kaifer AE, Stockdale D, Bazan GC. Electrochemical considerations for determining absolute frontier orbital energy levels of conjugated polymers for solar cell applications. Adv Mater 2011;23:2367–71. https://doi.org/10.1002/adma.201004554.
[34] He Q, Worku M, Liu H, Lochner E, Robb AJ, Lteif S, Vellore Winfred JSR, Hanson K, Schlenoff JB, Kim BJ, Ma B. Highly efficient and stable perovskite solar cells enabled by low-cost industrial organic pigment coating. Angew Chem Int Ed 2021;60:2485–92. https://doi.org/10.1002/anie.202012095.
[35] Rombach FM, Haque SA, Macdonald TJ. Lessons learned from spiro-OMeTAD and PTAA in perovskite solar cells. Energy Environ Sci 2021;14:5161–90. https://doi.org/10.1039/D1EE02095A.
[36] Hummelen JC, Knight BW, LePeq F, Wudl F, Yao J, Wilkins CL. Preparation and characterization of fulleroid and methanofullerene derivatives. J Org Chem 1995;60:532–8. https://doi.org/10.1021/jo00108a012.